Master in Photonics

MASTER THESIS WORK

IMAGING POLARIMETRY FOR BIO APPLICATIONS

Sara Aguado Guaita

Supervised by Dr. Oriol Arteaga, (UB)

Presented on date 30th August 2021

Registered at

Escola Tècnica Superior
d'Enginyeria de Telecomunicació de Barcelona

Imaging polarimetry for bio applications

Sara Aguado Guaita

Feman Group, Dep. Física Aplicada i Òptica, IN2UB, C/Martí i Franquès 1, Universitat de Barcelona, Catalonia, Spain

E-mail: sara.aguado@estudiantat.upc.edu

Abstract. Polarimetric imaging is especially interesting for the fields of biology and medicine due to the capability of this technique to emphasize certain abnormalities in tissue such as cancerous growths that can interact differently with polarized light. In the present work, the construction and performance of a Mueller Matrix imaging polarimeter working in visible and near infrared spectral ranges is described enabling its reproduction. The measurement of real samples is reported, showing the virtues of this technique while presenting different calculations to extract further data from the raw measurements.

Keywords: Imaging, Mueller Matrix, polarimetry.

1. Introduction

Polarization properties provide information about a sample under study that cannot be obtained analysing regular intensity images. Also, polarimetry is a light-based measuring technique which is highly desirable due to the fast, manipulable, non-invasive and non-destructive nature of visible radiation.

In order to characterize a sample, different polarization elements such as retarders and polarizers must be conveniently employed. Knowing well these, the main polarization properties found in a sample, which are typically diattenuation, depolarization and birefringence or retardation, can be determined [1]. Diattenuation is usually governed by the absorption coefficient encountered by the different directions of polarization of light, something that is known as dichroism, although it can be also contributed by other forms of extinction. Moreover, depolarization responds to a reduction on the polarization degree of light due to scattering in a certain media which results in a loss of coherence. Finally, a phase difference between two polarization states caused by the propagation of light in a sample is quantified as the birefringence or retardation value. Depolarization and retardation are the most common properties when referring to biological tissue due to the presence of tissue anisotropy and multiple scattering effects.

Concerning biomedical applications, research on imaging polarimetry has experienced lately an increasing interest as it provides contrast to discriminate between healthy and damaged tissue. Several polarization-related optical techniques are being used in the biomedical field. Some of them are Orthogonal Polarization Spectral [2], where the incident light is orthogonally polarized with respect to the detected light, Stokes vector polarimeters [3] and Mueller Matrix polarimeters, which is the technique discussed in this work.

When light interacts with biological tissue its direction of polarization is changed mainly by the multiple scattering events undergone by the photons and the local birefringence of some parts of the tissue. Therefore, the analysis of a polarimetric image can provide information about the organization of different layers constituting the sample or information about their composition

and thickness. Biological tissue can be roughly divided in weakly scattering, mainly found in liquids or transparent media, and strongly scattering media. It should be considered that the measurements in this last case correspond to an average of the multiple events experienced by light in its travel through tissue [4].

Special attention should be paid to what is called the Near Infrared (NIR) window. Light in the 650-1350nm wavelength range penetrates deeper in tissue and therefore, inner parts of it can be examined. This is due to the low absorption and scattering coefficients of blood and skin at such wavelengths while water's absorption is still moderate [5].

The instrument here presented obtains complete Mueller Matrix images in the NIR and visible ranges. It operates in reflection and close to normal-incidence (back-scattering configuration). This is highly desirable for bio applications since the sample does not need to be partially transparent for the detector to collect the required amount of light, as it occurs in transmission configurations.

2. Theoretical frame

Polarization of light can be described mathematically by means of the Stokes vectors and Mueller matrices (MM). Stokes vectors, $\mathbf{S}$, are four element vectors that describe the state of polarization of light through radiometry measurements. The first element (S_0) corresponds to the total intensity of light, while the rest of the elements result from the subtraction of horizontal and vertical linearly polarized light components (S_1), 45º and 135º linearly polarized light components (S_2) and right and left circularly polarized light components (S_3). For completely depolarized light, only S_0 is different from zero. The directions of polarization are determined with respect to a certain coordinate system previously fixed and the normal to it is typically the direction of the light propagation. 4x4 Mueller matrices, $\mathbf{M}$, characterize the sample properties by means of 16 real elements that transform Stokes vectors according to $\mathbf{S_{out}} = \mathbf{M}\,\mathbf{S_{in}}$. These matrices can be determined by analyzing the Stokes vectors of the ingoing and outgoing light after interacting with the sample, which is the job done by Mueller matrix polarimeters [1]. Instruments that determine the MM can use different setup configurations such as those containing Liquid Cristal devices [6], polarization gratings [7], or photoelastic modulators [8]. The instrument presented in this work conforms a dual rotating compensator Mueller Matrix polarimeter with imaging capabilities.

In order to control the polarization directions of light sent and collected from the sample, a Polarization State Generator (PSG) and a Polarization State Analyzer (PSA) are commonly placed enclosing the sample. The PSG is composed of a polarizer and a retarder and the PSA is analog, but the light crosses firstly the retarder and lastly the polarizer. Moreover, the different polarization states are acquired by rotating the retarders to a set of predetermined angles and measuring the intensity for each angular setting. The minimum number of discrete angles to determine the full MM is 16. This rotation can also be performed in a continuous fashion where the speed is a constant along the measurement but different for each retarder and the initial orientation of the fast axis is known [9]. Nevertheless, this configuration requires an average over a considerable number of measurements in order to obtain well-conditioned results. As for imaging applications the matrix multiplications are performed for every pixel of the camera, the fact that discrete rotation only operates with 16 angles will diminish the acquisition and computing time [10]. At the final stage, the calculation of the light intensity reaching a detector is obtained from the following calculation:

$$\mathbf{S_{out}} = \mathbf{P_2}\,\mathbf{M_{R2}}\,\mathbf{M_S}\,\mathbf{M_{R1}}\,\mathbf{P_1}\,\mathbf{S_{in}} \qquad (1)$$

Where $\mathbf{P_1}$ and $\mathbf{P_2}$ are the Stokes vectors of the two static polarizers, $\mathbf{S_{in}}$ and $\mathbf{S_{out}}$ are the Stokes vectors of the incident and exiting light, $\mathbf{M_S}$ is the Mueller matrix of the sample (which will be determined by the instrument) and $\mathbf{M_{R1}}$ and $\mathbf{M_{R2}}$ are the Mueller matrices for the rotating retarders. Said Mueller matrices vary depending on the rotation angles according to:

$$\mathbf{M_R} = \mathbf{R}(-\theta)\,\mathbf{M_C}\,\mathbf{R}(\theta), \tag{2}$$

where:

$$\mathbf{R}(\theta) = \begin{pmatrix} 1 & 0 & 0 & 0 \\ 0 & \cos(2\theta) & \sin(2\theta) & 0 \\ 0 & -\sin(2\theta) & \cos(2\theta) & 0 \\ 0 & 0 & 0 & 1 \end{pmatrix} \tag{3}$$

$$\mathbf{M_C} = \begin{pmatrix} 1 & 0 & 0 & 0 \\ 0 & 1 & 0 & 0 \\ 0 & 0 & \cos(\delta) & -\sin(\delta) \\ 0 & 0 & \sin(\delta) & \cos(\delta) \end{pmatrix} \tag{4}$$

Where θ is the angle of rotation of the fast axis and δ is the retardance of the compensator.
Since all parameters described in Eq. 1 are known except for the 16 elements of $\mathbf{M_S}$, the coefficients multiplying each MM element can be grouped into what is called the Basis vector ($\mathbf{B}$) [9].

$$\mathbf{B} = \begin{pmatrix} 1 \\ \cos^2(2\theta_0) + \cos(\delta_0)\sin^2(2\theta_0) \\ \cos(2\theta_0)\sin(2\theta_0)(1 - \cos(\delta_0)) \\ \sin(\delta_0)\sin(2\theta_0) \\ -(\cos^2(2\theta_1) + \cos(\delta_1)\sin^2(2\theta_1)) \\ -(\cos^2(2\theta_0) + \cos(\delta_0)\sin^2(2\theta_0))(\cos^2(2\theta_1) + \cos(\delta_1)\sin^2(2\theta_1)) \\ -\cos(2\theta_0)\sin(2\theta_0)(1 - \cos(\delta_0))(\cos^2(2\theta_1) + \cos(\delta_1)\sin^2(2\theta_1)) \\ -(\sin(\delta_0)\sin(2\theta_0))(\cos^2(2\theta_1) + \cos(\delta_1)\sin^2(2\theta_1)) \\ -\cos(2\theta_1)\sin(2\theta_1)(1 - \cos(\delta_1)) \\ -(\cos^2(2\theta_0) + \cos(\delta_0)\sin^2(2\theta_0))(\cos(2\theta_1)\sin(2\theta_1)(1 - \cos(\delta_1))) \\ -(\cos(2\theta_0)\sin(2\theta_0)(1 - \cos(\delta_0)))(\cos(2\theta_1)\sin(2\theta_1)(1 - \cos(\delta_1))) \\ -\sin(\delta_0)\sin(2\theta_0)(\cos(2\theta_1)\sin(2\theta_1)(1 - \cos(\delta_1))) \\ \sin(\delta_1)\sin(2\theta_1) \\ \sin(\delta_1)\sin(2\theta_1)(\cos^2(2\theta_0) + \cos(\delta_0)\sin^2(2\theta_0)) \\ \sin(\delta_1)\sin(2\theta_1)(\cos(2\theta_0)\sin(2\theta_0)(1 - \cos(\delta_0))) \\ \sin(\delta_0)\sin(2\theta_0)\sin(\delta_1)\sin(2\theta_1) \end{pmatrix} \tag{5}$$

Where $\theta_0, \theta_1, \delta_0$ and δ_1 are the angles of rotation and retardances of the compensators in the PSG and PSA, respectively.
If one considers a collection of N different intensity measurements corresponding to different angular settings, the Basis vector can be converted into a Nx16 matrix. This matrix describes the polarization effects of the retarders and polarizers as well as the incident light for the whole set of 16 angles [9]. The intensity captured by the camera for each angular setting of the PSG and PSA is arranged in a vector ($\mathbf{I}$) with N components that is given by $\mathbf{I} = \mathbf{BA}$, where $\mathbf{A}$ is a vector of 16 components that contains the 16 MM elements.

Therefore, the MM elements describing the sample properties at each pixel of the camera can be obtained using an inversion process. If $N=16$ it is possible to directly obtain the Mueller matrix elements from $\mathbf{A} = \mathbf{B}^{-1}\mathbf{I}$. In the more general case where $N > 16$, the following equation is used to find the MM elements [9]:

$$\mathbf{A} = (\mathbf{BB}^T)^{-1}\mathbf{BI} \tag{6}$$

where $\mathbf{BB}^T$ is a matrix of dimension 16x16 which must be invertible in order to solve Eq. (6). This condition is fulfilled when the value of the determinant is not zero, i.e. when the matrix is

not singular. In fact, the larger the determinant the better, as the measurement becomes better conditioned and more resilient against noise. For N=16, instead of checking the value of the determinant, one can also analyze the condition number of **B** and it has been discovered that the condition number of **B** must ideally be equal to the square root of 3 [11].

An advantage of MM measurements with respect to other techniques involving polarized light measurements is that there is no need to rotate the sample in order to obtain its complete polarization properties. Sample rotation in the back-scattering configuration can be calculated with the following simple matrix multiplication [13]:

$$\mathbf{M}_X = \mathbf{R}(\alpha)\, \mathbf{M}_{\text{Rec}}\, \mathbf{R}(\alpha), \tag{7}$$

where α is the angle of rotation of the sample and $\mathbf{M}_{\text{Rec}}$ is a Mueller matrix corresponding to the back-reflection configuration. This MM has some special properties since, in this configuration, a swap in the ingoing and outgoing beams has no effect on the sample's MM. Mueller Matrices with said properties are known as Reciprocal MM, and lead to the following symmetries [13]:

$$\mathbf{M}_{\text{Rec}} = \begin{pmatrix} m_{00} & m_{01} & m_{02} & m_{03} \\ m_{01} & m_{11} & m_{12} & m_{13} \\ -m_{02} & -m_{12} & m_{22} & m_{23} \\ m_{03} & m_{13} & -m_{23} & m_{33} \end{pmatrix}. \tag{8}$$

Any MM measured in a strict back-scattering configuration should obey these symmetries. However, in a real instrument (for instance, the one discussed in the next section) as there is still a small inevitable angle of incidence, some small deviations from these symmetries are possible.

In general, it should be noted that MMs are highly sensitive to small changes in the azimuth of the anisotropic properties. For example, the rotation shown in Eq. (7) makes that certain elements in $\mathbf{M}_X$ depend on 4α. Mueller matrices are generally presented normalized to the first element m_{00} so that the values of the elements can range between -1 and 1.

3. Method

The instrument built during this Thesis is an imaging Mueller Matrix polarimeter mounted vertically and in back-reflection mode, meaning that the polarization generation and analysis are distributed in two independent arms forming a V shape targeting the sample. In Figure 1, an image of the setup is shown, and it is further described in the next paragraphs.
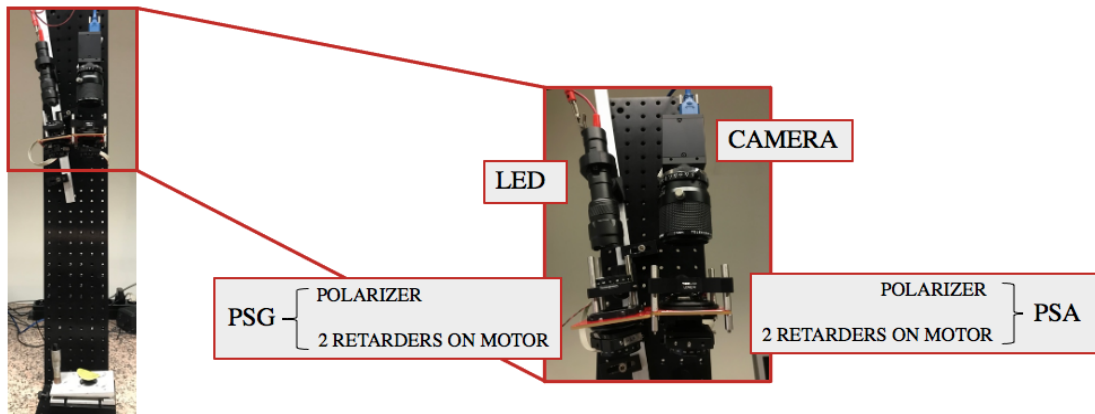

Figure 1. Scheme of the imaging MM polarimeter built with further detail on the body of the setup.

The light source is placed at the top of the structure. The system works for visible wavelengths as well as for near infrared (NIR) wavelengths with the purpose of imaging deeper in tissue. For the first case, a green LED (Green Focusing Waterproof LED flashlight, UltraFire) is employed and, when it is convenient, it is exchanged by a LED emitting in the NIR (Focusing Infrared Night

Vision Flashlight, UltraFire). The setup was calibrated for 500, 850 and 940nm wavelength light sources. Both NIR light sources include a collimator lens in order to collect the light and transmit it in quasi-parallel to the optical axis. For some highly reflective samples (e.g. a mirror) the light intensity provided by the LEDs is too high and a diffusor must be placed next to it. In principle, any light source could be suitable, but the use of incoherent LEDs avoids speckles and it is also the cheapest option.

The polarimetric components of the setup are contained in two main parts: a Polarization State Generator (PSG) and a Polarization State Analyzer (PSA). Both structures contain a polarizer and two retarders which are mounted on a rotating motor.

The polarizers selected work properly for both visible and NIR wavelengths. In particular, a polymer film polarizer (Edmund Optics) converts the incoherent and unpolarized light coming from the LED into linearly polarized light. This type of polarizer is preferable in terms of weight and aperture size over the ones made of crystal. Reflective wire grid polarizers (Edmund Optics) were also tested. Nevertheless, it was found that back and forth light reflection between the two polarizers contained in the setup distorted the MM measurements, so their use was discarded. The orientation of polarizers can be random as long as it is well known. Further, a crossed configuration is useful for the calibration due to the fact that it can be well determined since the two polarizers are perfectly perpendicular and the intensity captured by the camera becomes minimum.

For the compensators, 90° polymer film retarders are employed commonly since they are easy to find, have a low price, a large aperture and work acceptably well for this application. Their effect on polarized light is a delay of $\lambda/4$ in the phase of one of the polarization components with respect to the perpendicular one. This occurs due to the birefringent properties of retarders, also known as waveplates, which means that due to the presence of two different indexes of refraction, the polarized components of light propagate at two different speeds. However, it is known that the ideal retardance for the waveplates included in rotating compensator MM polarimeters is 132° since it enables a minimization of the condition number of the basis factor [11]. The use of a customized Fresnel prism providing this value was contemplated. However, the price of this element is very high and its narrow aperture limits the usefulness for imaging applications. Also, 132° polymer film retarders are not found in the market so they would only be available custom-made, which implies a considerable increment in their price. In turn, according to Gottlieb and Arteaga in [11], two 90° polymer retarder films (WP140HE, Edmund Optics) misaligned by a certain angle reach the same conditions. The proper angle between the retarders varies depending on the wavelength of the light source.

Following the initial idea of a polarimeter that covers the visible and NIR range, one of the retarders is mounted in a precision rotation stage to allow the user to modify its azimuth orientation conveniently. For further ease, the program interface includes a numeric control where the light source's wavelength is typed and the amount of mutual rotation between the two retarders is provided. This is obtained from an interpolation of the measured retardance values versus the wavelength contained in a look-up table. Said values were obtained by means of a spectroscopic MM ellipsometer detailed by Bian, et al. in [10] and available in the laboratory. In essence, the new two-retarder configuration becomes an elliptical retarder as a result of the combination of a circular and a linear retarder [11].

In order to reach the 16 discrete angles to which the azimuth of the elliptical retarder must be oriented to calculate the MM of the sample, said retarder in PSA and PSG is rotated by a piezoelectric rotating motor (Rotation Mount: SM1 Threaded, Thorlabs).

Finally, the light is detected by a USB 3.0 Monochrome camera (1/1.8", Edmund Optics) sensitive to visible and NIR light which is attached to a telecentric objective lens (2/3" 55mm C Mount, Computar). The selected FOV for the measurements is about 5 cm but depends on the objective's focus position which can be modified to focus at 140mm-Infinity. An alternative configuration in

which the objective of the camera was placed between the PSA and the sample was also considered. However, it was discarded as an additional lens was required to focus the image on the sensor, complicating the design and resulting in a poor image quality. Also, the measurement was misrepresented due to the fact that the objective lens could also introduce a certain change in polarization. Therefore, the chosen compact camera configuration only penalizes the results in terms of intensity and in a negligible way since the light source is powerful enough.

A Labview 2019 program controls the whole measurement process and performs the calculations detailed in the previous section. The whole process is completed in about 16 seconds time.

4. Calibration

The presented instrument is quite sensitive to small variations in optical alignment, so special care should be taken when building it. The most relevant parameters for the calibration procedure are the retardance values and the offset angles of the compensators.

In a preliminary step, during the construction of the MM polarimeter, the instrument was mounted following the basic configuration explained in Section 3 except for the measurement mode, which was chosen to be in transmission since it allows to use the identity MM as a reference. In this configuration, it is easy to check that the polarizers were oriented perpendicularly to each other. As one of them is mounted on a precision rotation stage, the most correct relative position which corresponds to the minimum intensity at the camera is easily found. For the alignment of the polarizers, a better accuracy is attained increasing the camera exposure time to increase the visual perception of intensity. Then, the same procedure is repeated for one of the retarders at the PSA and PSG in order to find the position where the polarization state is not changed when the polarized light crosses them. This is indicative that the fast axis of the compensator is coincident with the transmission/extinction axes of the polarizers. The same procedure is repeated for the second compensator. As the compensators are mounted on motorized rotation stages, the process is done sending different commands to the motors. Once the correct position is found, the degrees travelled by the motors are subtracted to the set of 16 discrete angles. Moreover, the direction in which the motors turn is checked to be correct by observing the intensities given by the camera at the 16 positions and comparing to the theoretical calculated values from (6).

The Labview program that controls the instrument contains an automatic calibration routine. This is capable of performing an automatic calibration either using an "air sample", when working in transmission [MM diag(1,1,1,1)], or using a mirror [MM diag(1,1,-1,-1)], when working in back-reflection, as reference sample. The calibration routine uses the mean intensity of all pixels in the image. Moreover, the calibration parameters considered by the routine are the retardance of the waveplates, the angles between each pair of retarders and the position offsets of the motors. Some initial values for these parameters need to be typed in the program, according to the preliminary knowledge that we have about the compensators. These initial guesses will usually be reasonably good approximations to the real values because we have a good knowledge about the characteristics of the compensators. However, in most cases, they will not be fully accurate, which means that the measured MM will not correspond directly to the identity matrix. In these cases, the optimization process must be implemented by a differential evolution algorithm that searches for the most accurate solution. This method minimizes the difference between the perfect identity matrix and the measurement by means of varying slightly said polarization values in a certain range. Other parameters such as the angle between the two polarizers could be modified, although an excessive number of degrees of freedom in the optimization usually leads to several possible solutions and wrong calibration outcomes. Therefore, it is preferable to fix the values of the calibration parameters that are well known; in particular, the retardance of the compensators, which we determined accurately using a MM ellipsometer [10]. The calibration process must be done each time the light source is changed or any aspect of the setup is modified.

One should also check that the image is not saturated, in order to obtain plausible results. In transmission, the detected intensity when there is no sample is given by:

Imaging polarimetry for bio applications

$$I = 1 - (\cos^2(2\theta_0) + \cos(\delta_0)\sin^2(2\theta_0))(\cos^2(2\theta_1) + \cos(\delta_1)\sin^2(2\theta_1)) - (\cos(2\theta_0)\cos(2\theta_1)\sin(2\theta_0)\sin(2\theta_1))(1 - \cos(\delta_0))(1 - \cos(\delta_1)) + \sin(\delta_0)\sin(\delta_1)\sin(2\theta_0)\sin(2\theta_1) \quad (9)$$

In Figure 2, the MM image of a leaf measured in back-scattering and the corresponding Standard Deviation, after averaging 10 successive measurements, is shown. The noise in the measurement is proved to be less than 0.02 for all MM elements.
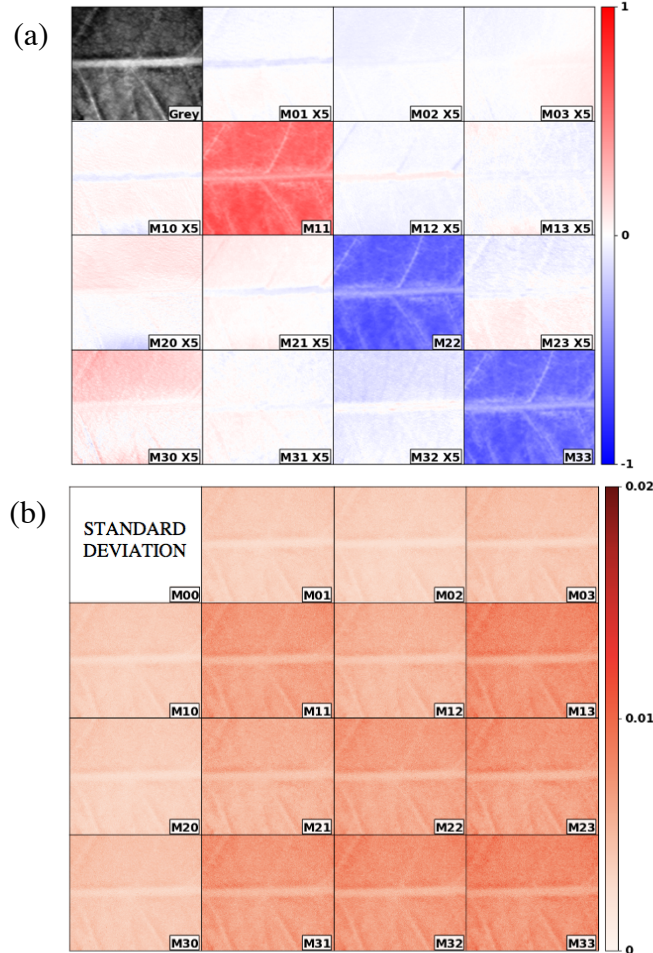

Figure 2. Measurement (a) and Standard Deviation (b) of the MM of a leaf measured at 550 nm.

5. Results

The MM measurements contain the polarimetric information of the sample in a quantitative way, but the interpretation of this data is not always straightforward. Some additional calculations of the results, such as the differential analysis [12], can be done. These can provide explicit polarimetric quantities as are retardances and diattenuations, that eventually can be related to structural features of the tissue. In this section, a selection of measurements performed with the imaging instrument that has been built will be discussed.

A comparison between a human finger illuminated by visible (a) and NIR (b) light sources is shown in Figure 3. Both images are MM measurements obtained in-vivo. The scale has been enhanced by a factor of 5 for off diagonal values since the result in these elements is very subtle. This is due to the weak polarization properties of bio samples. The fact that these small values can be still measured proves the high sensitivity of the setup. Also, the m_{00} element (that would be 1 for normalized MMs) has been replaced by the intensity image which corresponds to the mean of the 16 images obtained. Note that both MMs, show approximately the symmetries described in Eq. (8).

As light penetrates deeper in the NIR, the depolarization observed is larger due to the higher number of scattering events that randomize the polarization. This can be readily observed in the diagonal values which are closer to zero than in the visible image.
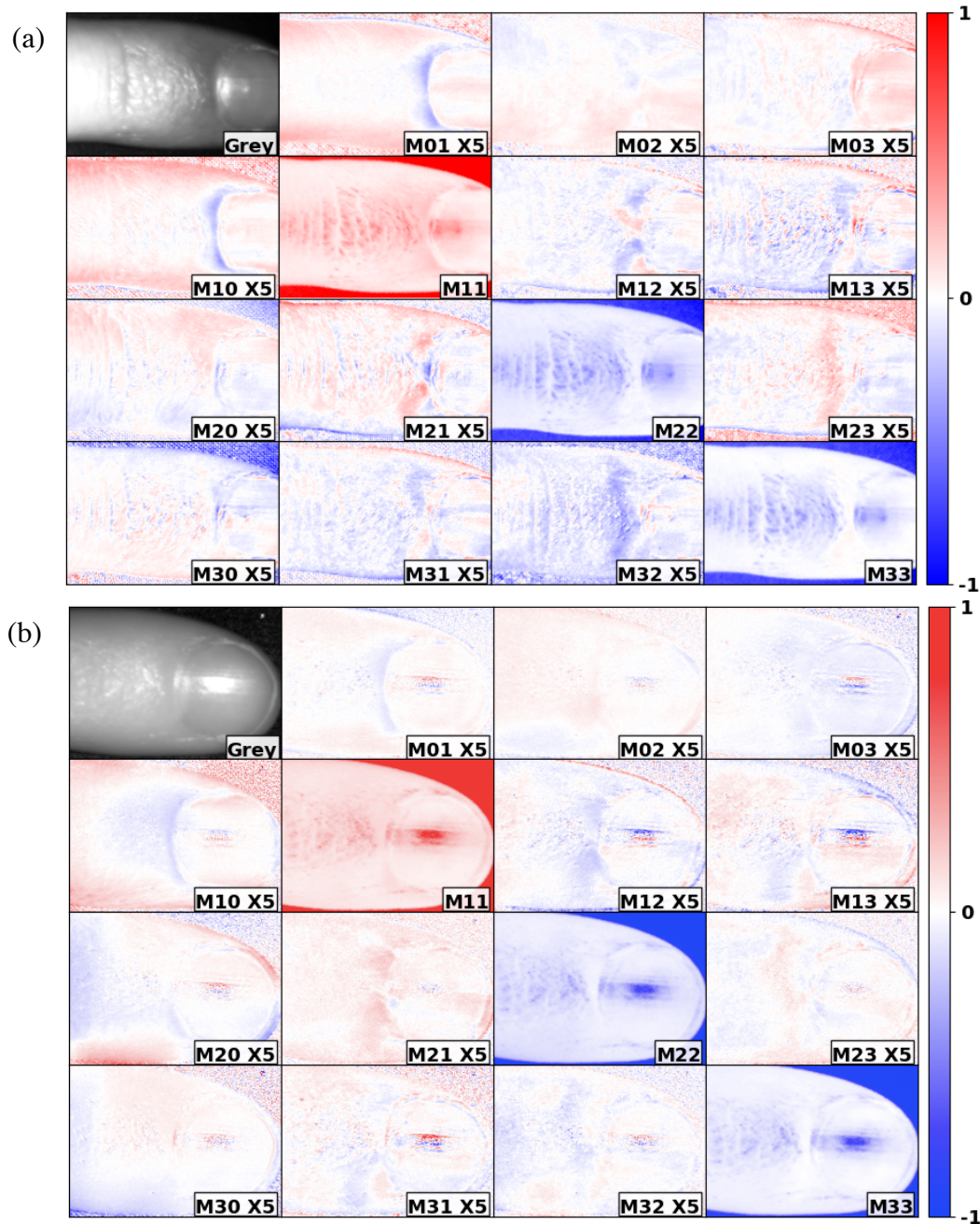

Figure 3. MM image of a human finger: (a) 25x20mm ROI obtained with 550 nm wavelength light source, (b) 20x16mm ROI obtained with 850 nm wavelength light source.

In (a), the effect of the polarization properties is more evident than in (b). For instance, a noticeable diattenuation is shown in elements m_{01} and m_{10} at the proximal nail fold region. This could be explained, although it is a mere assumption due to the lack of research on the subject, by the presence of very tiny and parallel capillaries acting as a polarizer as Mathura et al. discussed [2]. Further, m_{12} and m_{21} elements show different colors (painted in blue and red) that correspond to different orientations of linear retardation which could give some idea of a fibrillar tissue organization in the region. As explained in Section 2, this change in orientation does not need to be strong to be detected by the setup.

Figure 4 shows another measurement made in the back of a human hand where a skin scar was visible. This data was collected using 550nm wavelength light. In this case, instead of showing the raw MM images, the values of Linear diattenuation (b), Linear Birefringence (or retardation)

(d) and the angle of said Linear Birefringence (e) calculated from the differential MM analysis were plotted. Briefly, this analysis consists of taking the logarithm of the MM and studying the symmetries of the so-called differential MM [13]. In addition to these parameters, Fig. 4 also shows the intensity image (a) and Depolarization Index (c) calculated from:

$$DI = \sqrt{\frac{1}{3m_{00}^2}\left(\sum_{i,j=0}^{3} m_{ij}^2 - m_{00}^2\right)} \qquad (10)$$

Where DI = 0 means that the sample is fully depolarizing, which would be indicative that no polarization would survive after the interaction with the sample. Further details about DI can be found in [13].
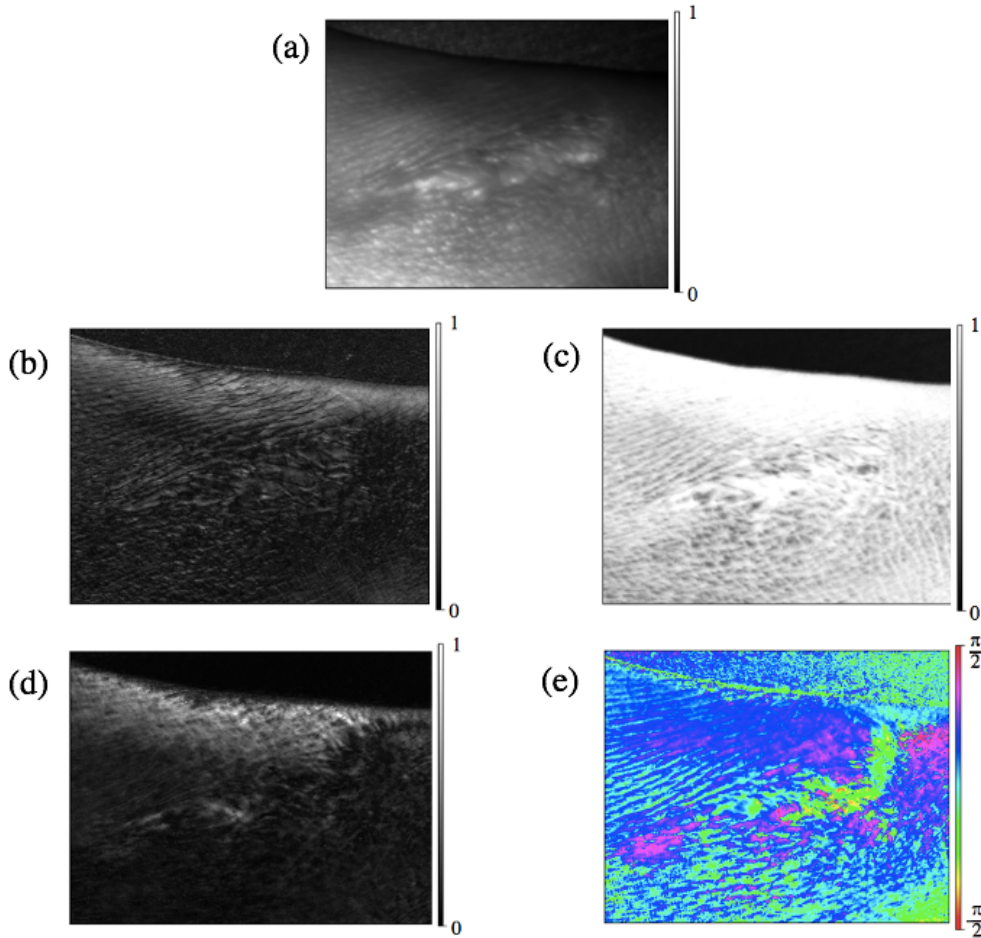

Figure 4. Polarimetric analysis of a scar on human skin tissue: (a) Intensity image, (b) magnitude of Linear Diattenuation, (c) Depolarization Index, (d) magnitude of Linear Birefringence, (e) Angle of Linear Birefringence. The real dimensions of the image correspond to 30x30 mm.

It is observed that the scar region presents a slightly larger value of DI than the surrounding skin. This is probably indicative that the penetration depth of light is shallower in the scar region. Also, the angle of LB in the scar is clearly distinct from the surrounding skin and it shows a much less homogenous trend, which is probably indicative that the collagen fibres have grown in different directions to heal the injury. It has been reported that, locally, the collagen fibers constituting scars are disposed in a more parallel fashion than in other tissues [14]. Therefore, they can have relatively large values of LB but cannot follow the same long-range order observed in the surrounding regions. For all that has been exposed, the setup is suitable for tracing healed or differently organized areas in biological tissue.

6. Conclusion
Information about polarimetric properties in biomedical samples is a step further for diagnostic, surgical and treatment monitoring procedures. As proven in this work, the MM imaging

polarimeter developed is capable of discerning even subtle details from real biological samples. Also, enabling the choice of the most convenient light source, it works both in the visible and NIR wavelengths. In a compact, cheap and easy-to-use configuration, the described setup acquires reliable results. Besides, MM measurements can be further analyzed performing different well-known matrix decompositions and algebraic methods to extract a large amount of polarimetric data about the sample. On the basis of these results, the instrument built can be used to learn the organization and composition of biological tissues in a noninvasive manner. Lastly, one can anticipate that a way to improve a limiting aspect of the setup for in-vivo measurements, which is the acquisition time, could be the replacement of the rotating stage with a faster option.

References

[1] Chipman R A 1994 Polarimetry in *Handbook of optics*, ed Michael Bass (New York: McGraw-Hill)

[2] Mathura K R, Vollebregt K C, Boer K, De Graaff J C, Ubbink D T and Ince C 2001 Comparison of OPS imaging and conventional capillary microscopy to study the human microcirculation *Journal of Applied Physiology* **91** 74-78

[3] Sabatke D S, Descour M R, Dereniak E L, Sweatt W C, Kemme S A and Phipps G S 2000 Optimization of retardance for a complete Stokes polarimeter *Optics letters* **25** 802-804

[4] Miller K 2011 *Biological and medical physics, biomedical engineering,* ed Elias Greenbaum (New York: Springer)

[5] Upputuri P K and Pramanik M 2019 Photoacoustic imaging in the second near-infrared window: a review *Journal of biomedical optics* **24** 40901

[6] Garcia-Caurel E, De Martino A and Drevillon B 2004 Spectroscopic Mueller polarimeter based on liquid crystal devices *Thin Solid Films* **455** 120-123

[7] Kudenov M W, Escuti M J, Hagen N, Dereniak E L and Oka K. 2012 Snapshot imaging Mueller matrix polarimeter using polarization gratings *Optics letters* **37** 1367-1369

[8] Arteaga O, Freudenthal J, Wang B and Kahr B 2012 Mueller matrix polarimetry with four photoelastic modulators: theory and calibration *Applied optics* **51** 6805-6817

[9] Arteaga O, Baldrís M, Antó J, Canillas A, Pascual E and Bertran E 2014 Mueller matrix microscope with a dual continuous rotating compensator setup and digital demodulation *Applied Optics* **53** 2236-2245

[10] Bian S, Cui C and Arteaga O 2021 Mueller matrix ellipsometer based on discrete-angle rotating Fresnel rhomb compensators *Applied Optics* **60** 4964-4971

[11] Gottlieb D and Arteaga O 2021 Optimal elliptical retarder in rotating compensator imaging polarimetry *Optics Letters* **46** 3139-3142

[12] Yoo S H, Ossikovski R and Garcia-Caurel E 2017 Experimental study of thickness dependence of polarization and depolarization properties of anisotropic turbid media using Mueller matrix polarimetry and differential decomposition *Applied Surface Science* **421** 870-877

[13] Arteaga O and Ossikovski R Mueller matrix analysis, decompositions and novel quantitative approaches to processing complex polarimetric data in *Polarized light, clinical and pre-clinical applications* (New York: Springer) (Publication pending)

[14] Van Zuijlen P P, Ruurda J J, Van Veen H A, Van Marle J, Van Trier A J, Groenevelt F and Middelkoop E 2003 Collagen morphology in human skin and scar tissue: no adaptations in response to mechanical loading at joints *Burns* **29** 423-431